Thiol-ene biobased networks: Furan allyl derivatives for green coating applications

THIOL-ENE BIOBASED NETWORKS: FURAN ALLYL DERIVATIVES FOR GREEN COATING APPLICATIONS

Lorenzo Pezzana [1], Giuseppe Melilli [2], Pierre Delliere [2], Dumitru Moraru [1], Nathanael Guigo [2], Nicolas Sbirrazzuoli [2], Marco Sangermano [1]

[1] *Dipartimento di Scienza Applicata e Tecnologia, Politecnico di Torino, C.so Duca degli Abruzzi 24, 10129, Torino, Italy*
[2] *Université Côte d'Azur, Institut de Chimie de Nice (ICN), UMR CNRS 7272, 06108, Nice Cedex 02, France.*

Corresponding authors: Nicolas.Sbirrazzuoli@univ-cotedazur.fr, marco.sangermano@polito.it

ABSTRACT:
Biomass feedstocks are playing a crucial role toward the development of new sustainable materials with the aim to replace the fossil-based ones limiting the emissions and waste. Among the other, cellulose, and hemicellulose are gaining interest as a source of new bio-based building blocks such as furan derivatives. In this study, two furan derivatives were selected as bio-based monomers to design four innovative UV-curable coatings. Specifically, 2,5-Furandimethanol (FDM), and cis-cyclobutane-1,2-dicarboxylic acid (CBDA-2) derived from Furylacrylic acid were modified by allylation of their respective OH groups. The bis allyl derivatives were combined with commercial tris- and tetra-functional thiols compounds and cured by means of UV-light through a thiol-ene reaction. The UV-curing was deeply investigated by means of real-time FT-IR, photo-DSC and photorheology. Successively, the bio-based thermosets were characterized by DMTA and tensile test to examine the thermal-mechanical behavior. The results indicated comparable properties with previous studied bio-based thiol-ene thermoset raising the possibility to use the studied material for coating applications.

KEY WORD: thiol-ene chemistry, UV-curing, furans, bio-based monomers, [2+2] cycloaddition

1. INTRODUCTION

Nowadays, green and sustainable are two approaches deeply investigated in material science to cope with environmental climate change and depletion of fossil resources. Most of commercially available products are currently fossil-based but researchers begin to pay considerable attention to bio-based materials and sustainable processes [1]. However, a rational alternative to replace petrochemical materials should be addressed in order to propose new bio-based building blocks that possess both competitive performances, as well as production cost. The large availability of by-products of the food industry, agriculture waste and forestry residue have encouraged the use of derivatives of lignin, cellulose and hemicellulose to develop a new array of biobased building blocks [2,3]. The use of such building blocks are gaining competitiveness in terms of industrial and socio-economic features with respect to the standard and well known sources and processes [4,5].
Among these building blocks, furan-based monomers have gained great attention due to the possibility to develop new polymers that can fulfill multiple applications [6,7] in particular due to their particular aromatic structure. Plant-based saccharides represent the raw material to produce furan derivatives, in particular, 5-hydroxymethyl furfural and furfural are two interesting platform molecules to produce biochemicals and several interesting monomers [8,9].

C6 sugar units and polysaccharides can be converted into hydroxymethyl furfural, whereas furfural can be produced starting from polysaccharide of C5 glycosidic unit, as shown in Figure 1.

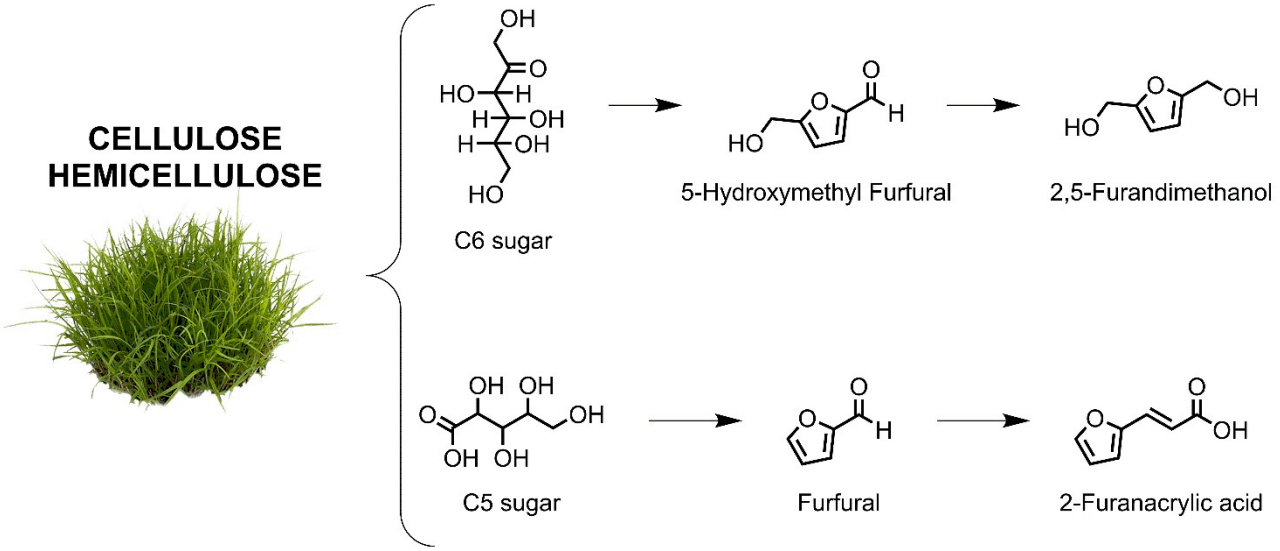

Figure 1. Derivatives from cellulose and hemicellulose: pentose and hexose sugar units.

Both compounds are characterized by interesting functional groups such as aldehyde. According with the aldehyde chemistry a vast array of reactions might be employed to easily modify hydroxymethyl furfural and furfural into specific monomers with the aim to satisfy different requests in term of polymer properties [4,10–12]. For example, furfuryl alcohol has been deeply studied due to the wide range of properties associated with its furan structure that can enhance the rigidity of the final polymer [13,14]. Furan dimethanol (FDM) is also an interesting starting point to develop several monomers. Different epoxy networks derived from FDM have been studied and characterized [15,16]. Furthermore, furan dicarboxylic acid (FDCA) is an example of well-known derivative and it has been used to make green polyester trying to substitute PET [17–19]. Moreover, poly(ethylene 2,5-furandicarboxylate) (PEF) can compete with traditional PET regarding price, performance as well as sustainability issues [20].

A new attracting category of material is cyclobutane dicarboxylic acids (CBDA-2) due to the special aliphatic ring (i.e. cyclobutane) present in its chemical structure. Furfural-derived trans-3-(2-furyl)acrylic acid [21] has been recently used to produce CBDA-2 under exposition to UV-light [22]. The UV-light is used to activate the so called [2+2] cycloaddition to link two units creating a new monomer. The special feature of this cycloaddition is the possibility to be reversible according to the wavelength used to irradiate the monomers [23–25]. Thus, it is possible to form or to destroy the ring in relation to the requirement.

CBDA-2 found applications as building block for polyesters [26], but it has also been used as cross-linker for epoxy vegetable oil revealing high tensile strength and a high glass transition of the final material [27]. Thus, it can be used as green cross-linker to produce complete biobased thermoset with similar properties to fossil derived thermoset.

Among the techniques used to cure thermoset polymers, UV-light assisted process occupied an important place. In fact, this technique reveals several advantages, among the others, the high curing rate, the lack of VOCs emission and the possibility to use mild condition [28,29]. Different UV methods, from radical to cationic, can be used according to the UV-reactive groups, such as epoxy ring, acrylates, methacrylates, and vinyl group. Thiol-ene chemistry reveals an interesting starting point to exploit UV-curing. Its click feature allows to reach high conversion and the lack of oxygen inhibition gives the possibility to cure in straightforward set up [30–32]. Several biobased monomers have been already employed. Terpenes [33–35], isosorbide derivatives [36–38], ferulic acid [39], and also furan [40] are examples of these researches in which the biobased monomers were functionalized and exploited in the thiol-ene chemistry revealing good outcomes. Considering specifically the furan

derivative, the FDCA has been adapted to classic thiol-ene chemistry by functionalization of the acid groups with allyl alcohol. The curing was studied with five different thiol compounds, yielding an array of bio-based thermosets [40]. Recently, we have shown that furan derivatives are excellent candidate for cationic UV curable coatings with tunable properties [15,41], so in this study we investigate the UV-curing of thiol-ene network based on furan derivatives. In fact, despite the advantages of UV-assisted thiol-ene reaction, this technique has not been extensively applied to the furan derivatives especially for coating applications. In this study two different allyl monomers were synthetized starting from furan-based derivatives: FDM and CBDA-2. Two different bi-allylated compounds were synthetized starting from the aforementioned furan molecule on purpose to evaluate the efficiency and the performance of different backbone of furans. In order to exploit the thiol-ene chemistry two different commercial thiols were used. The evaluation of the influence of the thiol-functionality into the polymer network was studied comparing the properties of the tested formulations. A complete characterization study of the photocuring process was carried out using real-time FTIR to follow the conversion in function of the time. Photorheology and photo-DSC were employed to corroborates the FTIR data following the kinetics. Instead, DSC and DTMA analyses were carried out to have thermo-mechanical outcome of the produced material. Finally tensile test was performed on free film and the coating properties were also analyzed for the different formulations.

2. MATERIALS AND METHODS

2.1.MATERIALS

2,5-Furandimethanol (FDM) was purchased from Apollo Scientific (97 % purity); trans-3-(2-furyl)acrylic acid (FAA), allyl bromide, sodium hydroxide (NaOH), magnesium sulphate ($MgSO_4$), were purchased from Sigma Aldrich. Acetonitrile, dimethyl sulfoxide (DMSO), diethyl ether and dichloromethane (DCM) were provided by Carlo Erba. The deuterated DMSO (DMSO-d_6) for NMR analysis was supplied from Sigma.
The trimethylolpropane tris(3-mercaptopropionate) (TMPMP) and the pentaerythritol tetrakis(3-mercaptopropionate) (PETMP) were provide by Bruno Bock Gmbh and the photoinitiator, phenylbis(2,4,6-trimethylbenzoyl)phosphine oxide (BAPO), was provided by BASF.

2.2.SYNTHESIS OF 2,5-BIS((ALLYLOXY)METHYL) FURAN (BAMF)

Following and adapting previous protocols [42,43], FDM (3.00 g, 23.4 mmol) was weighted in a round bottom flask and dissolved in acetonitrile (150 mL). Pulverized NaOH was added (3.75 g) and the mixture was stirred for 30 min then allyl bromide (7.02 mL, 8.1 mmol) was slowly added at 0°C. The reaction was left for 3 days at room T. After the precipitate was filtered off and rinsed with acetonitrile. The solvent was evaporated and extraction with diethyl ether was performed. The water layer was extracted three times. The collected organic phases were washed with water and dried over $MgSO_4$. The solvent was removed under reduced pressure and the product was used without other purification (3.96 g, yield 81 %). The **Scheme 1** reports the chemical reaction.

^{1}H NMR (400 MHz, DMSO-d_6) δ 7.67 – 7.62 (m, 2H), 6.43 (d, J = 1.7 Hz, 4H), 5.88 (ddt, J = 17.3, 10.6, 5.4 Hz, 2H), 5.26 (dq, J = 17.3, 1.8 Hz, 2H), 5.20 – 5.12 (m, 2H), 4.41 (s, 4H), 3.95 (dt, J = 5.4, 1.5 Hz, 4H).

Scheme 1. Allylation of furandimethanol by reaction with allyl bromide.

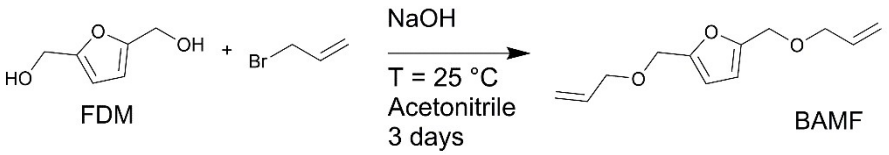

2.3.SYNTHESIS OF BISALLYL CYLOBUTANE DICARBOXYLATE (BACBDA)

The synthesis is a two-step reaction as shown in **Scheme 2**. The first step was done according to previous syntheses [27,44]. Furylacrylic acid (25 g, 181 mmol) was suspended in hexane (250 mL) in a 1000 mL flask. Strong mixing was provided, and two commercially available lights (50-watt black light) were used to provide the UV-irradiation. The reaction was left under the total conversion of the reagent by measuring it through ^{1}H-NMR. The solid product was filtrated through a filter G4 and then was left to dry overnight to remove all the hexane. The final brownish solid product (CBDA-2, 24 g, yield 97 %) was fully characterized by NMR (**Figure S1**).
The second step was done following other synthesis [45]. CBDA-2 (7.00 g, 25.4 mmol) was dissolved in DMSO (100 mL). NaOH (4.06 g) was pulverized and added into the solution. Then allyl bromide (8.78 mL, 10 mmol) was finally added. The reaction was left for 3 days at 50 °C. The reaction was stopped by decreasing the temperature. DCM was used to extract the organic product. Three extractions against water were performed. The collected organic phase was then washed with water and brine. Finally, it was dried over $MgSO_4$. The solvent was removed by evaporation under reduced pressure obtaining a viscus brown liquid as final product (8.5 g, yield 94 %).

^{1}H NMR (400 MHz, DMSO-d_6) δ 6.60 (d, J = 1.9 Hz, 2H), 5.47 – 5.27 (m, 4H), 5.14 – 5.00 (m, 2H), 4.58 – 4.32 (m, 4H), 3.80 – 3.66 (m, 4H), 3.36 – 3.25 (m, 2H), 3.07 (dq, J = 4.9, 1.6, 1.1 Hz, 2H).

Scheme 2. Synthesis of bis allyl CBDA-2 starting from trans-3-(2-furyl) acrylic acid with two steps protocol.

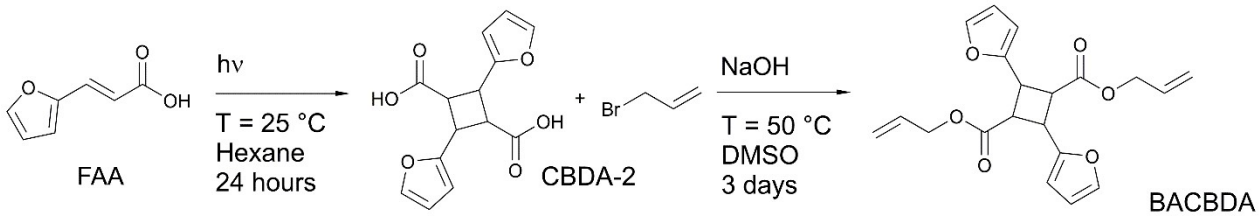

2.4. FORMULATION AND PHOTO CROSSLINKING

The synthetized allyl-monomers were mixed with two different commercially available thiols, the trimethylolpropane tris(3-mercaptopropionate) (TMPMP) and the pentaerythritol tetrakis(3-mercaptopropionate) (PETMP). The stoichiometric ratio between allyl group and thiol group was fixed at 1:1 to have the exact equivalent of both functional groups (ene and thiol) involved into the reaction. Finally, BAPO photoinitiator was added to the formulations. The chemical structure of the ene and thiol monomers with a schematic view of the UV-curing is reported in **Scheme 3**. The different formulations are listed in the **Table 1**. The three components, allyl monomer, thiol monomer and photoinitiator were mixed in an ultrasound bath until the BAPO was completely dissolved. The formulations were kept in brown vials to avoid light contact. Preliminary tests were carried out to assess the exact concentration of BAPO into the formulations. To do so, photocuring process was investigated varying the BAPO concentration from 0 to 3 phr (per hundred resin). Finally, the photoinitator was set at 3 phr to produce the specimens for the further characterizations. The formulations were spread on a Telfon substrate with a film bar ensuring a thickness of 150 μm. The photocuring was carried out by exposing the formulation to UV light for 5 min. A DYMAX flood

lamp was used as the UV-light source with the light intensity set around 130 mW/cm^2. The emission spectrum of the UV lamp was from 275 to 500 nm with a maximum located to 365 nm.

Scheme 3. Chemical structure of the monomers involved in the UV-curing and schematic view of the photocuring process. The illustration of UV-curing is done exploiting BAMF and TMPMP (green box).

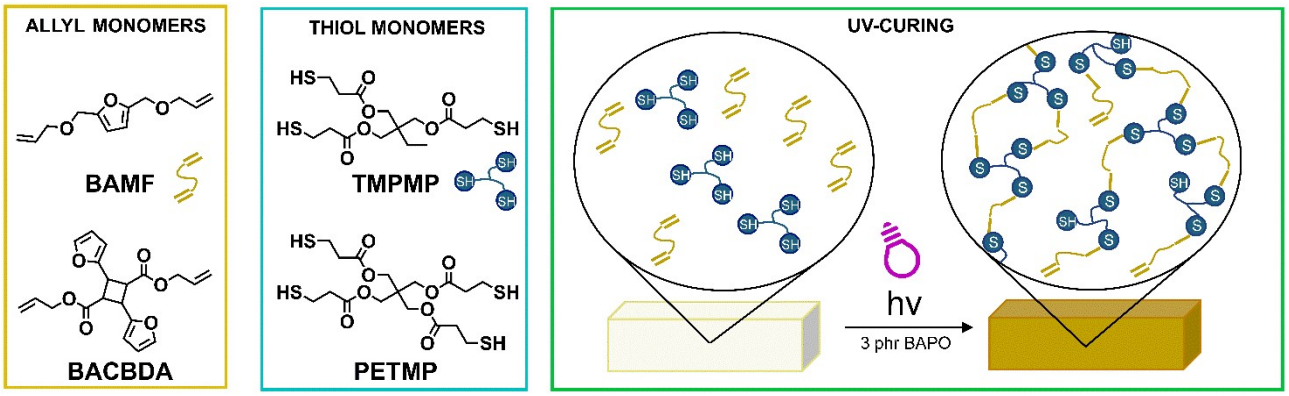

Table 1. Formulation tested in the study with the synthetized allyl monomer and the commercial thiols. The photoinitiator was added evaluating the total amount of the resin.

ENTRY	Allyl monomer	Mass (g) [mmol]	Thiol monomer	Mass (g) [mmol]
BAMF_TMPMP	BAMF	0.500 [2.4]	TMPMP	0.638 [1.6]
BAMF_PETMP	BAMF	0.500 [2.4]	PETMP	0.587 [1.2]
BACBDA_TMPMP	BACBDA	0.500 [1.4]	TMPMP	0.373 [0.9]
BACBDA_PETMP	BACBDA	0.500 [1.4]	PETMP	0.343 [0.7]

2.5. CHARACTERIZATION

2.5.1. NUCLEAR MAGNETIC RESONANCE (NMR)

NMR analysis was done by means of Brucher AM 400. Both ^{1}H-NMR (400 MHz) and ^{13}C-NMR (101 MHz) were conducted on the different products. DMSO-d_6 was used as solvent reference for all the analysis.

2.5.2. REAL-TIME FOURIER TRANSFORM IR (real-time FTIR)

The photo-curing process was followed by means of a Nicolet iS 50 Spectrometer. The formulations were spread on a silicon slice with a thickness of 32 μm by means of film bar. The spectra were collected with a spectral resolution of 4 cm^{-1}. All the data were handled by OMNIC software developed by Thermo Fisher Scientific.
The conversion curves were collected by monitoring the disappearance of the thiol peaks at 2570 cm^{-1} and the carbon-carbon double bond at 930 cm^{-1}. The peak at 1730 cm^{-1} was taken as reference. It was assumed to be unaffected by UV-irradiation since it belonged to the C=O bending of the ester that was not involved into the curing reaction. Equation 1 was used to calculate the conversion during the exposure time.

$$Conversion\ (\%)\ = \frac{\left(\frac{A_{fun}}{A_{ref}}\right)_{t=0} - \left(\frac{A_{fun}}{A_{ref}}\right)_{t}}{\left(\frac{A_{fun}}{A_{ref}}\right)_{t=0}} \times 100 \qquad \text{(Eq. 1)}$$

where A_{fun} is the area of the functional group under investigation (e.g. area of the thiol at 2860 cm^{-1}) while A_{ref} is the area of the peak at 1730 cm^{-1}. The evaluation is done at different interval of time to elaborate the conversion curve.

2.5.3. PHOTO DYNAMIC SCANNING CALORIMETRY (photo-DSC) and DYNAMIC SCANNING CALORIMETRY (DSC)

The photo-curing process was investigated by means of photo-DSC. A Mettler TOLEDO DSC-1 equipped with Gas Controller GC100 was used to perform the analysis. The DSC was equipped with a mercury lamp, Hamamatsu LIGHTINGCURE LC8, with an optic fiber to direct irradiate the samples. The emission of UV-light was centered at 365 nm. About 5-10 mg of photocurable formulation was placed in an open aluminum pan (40 ul), whereas an empty pan was used as reference. The tests were done at room temperature (25 °C) and in controlled atmosphere (N_2 flow of 20 mL/min). The samples were irradiated two times for 10 min in order to proper evaluate the UV-curing. The second run was done to confirm the complete curing and create the base line. The second curve was subtracted from the first to obtain the curve related to the curing only. The integration of this curve gave the final result. The final conversion was evaluated by exploiting the Equation 2.

$$Conversion\ (\%)\ = \frac{\Delta H_{exp}}{\Delta H_{theo}} \times 100 \qquad \text{(Eq. 2)}$$

The evaluation of the T_g of cured samples was done by means of dynamic scanning calorimetry; a Mettler TOLEDO DSC-1 was used. The DSC analysis was performed on samples of about 5-10 mg that were sealed in 40 µl aluminum pans and analyzed. The starting temperature was set as 25 °C; the first heating goes from 25 to 100 °C; after that the chamber was again cooled until – 50 °C was reached and finally was a second heating from – 50 °C to 300 °C applied. After each dynamic steps, isothermal step of 5 min were done to stabilize the chamber and the sample. The first heating was done in order to eliminate the thermal history of the polymers. The heating and the cooling rates were set at 10 °C/min and the analysis was performed in a N_2 atmosphere with a flow rate of 40 mL/min. All the data were analyzed with Mettler Toledo STARe software V9.2.

2.5.4. PHOTO-RHEOLOGY

The curing process was studied by means of photo-rheology. An Anton Paar MC 302 rheometer (Physica MCR 302, Graz, Styria). The rheometer was set with a plate-plate geometry, the outside diameter of the metal disk was 25 mm and a quartz disk was used as bottom support in order to guarantee the irradiation of the sample. The distance between the plate was set as 100 µm. 150 µL of the formulation were placed between the plates. The UV-light was provided by optic fiber to directly irradiate the sample. A Hamamatsu LIGHTINGCURE LC8 was used as UV-source. The light intensity provided on the surface of the sample was 40 mW/cm^2. The lamp was turned on after 60 second of stabilization and the measurements were performed in oscillatory condition at frequency of 1 Hz, with strain 1 % and in isothermal condition at room temperature.

2.5.5. GEL CONTENT

The gel content percentage (% gel) was evaluated on UV-cured samples. About 200 mg samples were tested, the curing was done using Teflon mold as describe in paragraph 2.4. The determination of gel content was done by evaluating the weight loss after 24 h extraction with chloroform at room

temerature. The samples after the immersion were allowed to dry for 24 h in air. The gel % was calculated according to Equation 3.

$$\% \, gel = \frac{W_1}{W_0} * 100 \quad \text{(Eq. 3)}$$

where W_1 is the weight of the dry film after the treatment with chloroform and W_0 is the weight of the dry sample before the treatment.

2.5.6. DYNAMIC MECHANICAL THERMAL ANALYSIS (DMTA)

The thermo-mechanical analysis of the thermosets was carried out with a Triton Technology instrument. The heating rate was set at 3 °C/min and the initial temperature of – 20 °C was achieved by cooling down the test chamber with liquid nitrogen. The instrument applied uniaxial tensile stress at frequency of 1 Hz. The measurement was done to detect the T_g as maximum of *Tan* δ curve and were stopped after the rubbery plateau. The samples were UV-cured in a silicon mold with average dimension of 0.2 x 3.5 x 12 mm. Equation 3 is derived from the statistical theory of rubber elasticity and gives an estimation of the density of cross-links.

$$\nu_c = \frac{E\prime}{3RT} \quad \text{(Eq. 4)}$$

where ν_c is the number of crosslinks per volume of the crosslinked network, E' is the storage modulus in the rubbery plateau (T_g + 50 °C), R is the gas constant and T is the temperature expressed in Kelvin.

2.5.7. TENSILE MEASUREMENTS

The mechanical properties of the thermoset were investigated by tensile test. The stress-strain curve was registered using a tensile instrument (MTS QTestTM/10 Elite, MTS System Corporation) combined with a measurement software (TestWorks® 4, MTS System Corporation). A 1 kN load cell was used, and the traverse speed of the machine was set as 5 mm/min [46]. The Young's modulus (E) was evaluated as the tangent of the curve up to the linear region (around 20 % of total elongation). The result was the average value of 5 measurements.

2.5.8. CONTACT ANGLE AND HARDNESS

In order to evaluate coating properties, such as contact angle and pencil hardness, the formulations were UV-cured on glass substrate with a thickness of 150 μm. The contact angle test was performed on the free surface with water. The instrument used was a Drop Shape Analyzer, DSA100, Krüss. The pencil hardness was measured according to the standard ASTM D3363 [47]. The hardness was measured by means of Sauter HMO mobile Leeb Hardness Tester. Five measurements were taken to have an average value.

3. RESULTS AND DISCUSSION

3.1.SYNTHESIS

The functionalization of furan monomers was done according to previous protocols adapting the best reaction conditions in order to obtain high yield and purity of the final products. The allylation of FDM was achieved by one step reaction. Allyl bromide was used as reagent and NaOH was used as base for the activation of the alcohol group present in the FDM. The ^{1}H-NMR analysis showed the presence of a pure product, BAMF, with characteristic peaks of the allyl functional group, named c,d,e in **Figure 2** (the ^{13}C-NMR spectrum of BAMF is reported in **Figure S1**).

Instead, the allyl derivative of CBDA-2 was obtained with two steps reaction. The first step was done to produce the cyclobutene ring starting from furylacrylic acid by exploiting the [2+2] cycloaddition triggered by UV-irradiation [27]. The characterization of the intermediate was done by NMR analysis (see **Figure S2**). After the formation of CBDA-2, the allylation was achieved by reacting the monomer with allyl bromide in presence of NaOH. The product of each reaction was confirmed by both ^{1}H-NMR and ^{13}C NMR analysis. The characteristic peaks related to the presence of the allyl group are named as f, g, h in **Figure 2** for the BACBDA (the ^{13}C-NMR spectrum is reported in **Figure S3**).
The two allyl-functionalized monomers were employed in thiol-ene photochemistry reaction to achieve UV-cured coatings.

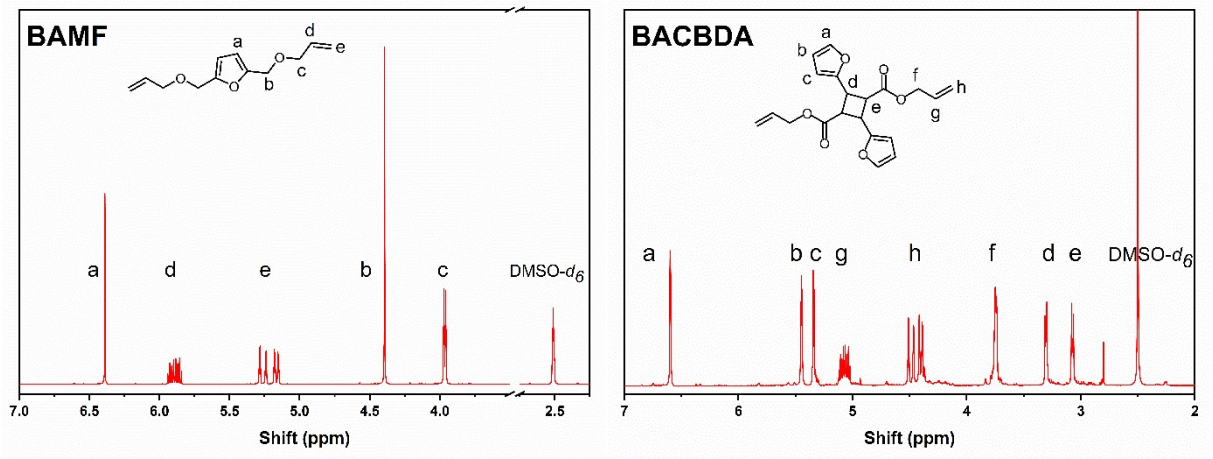

Figure 2. ^{1}H-NMR of the two bisallyl derivatives used for the thiol-ene study.

3.2. PHOTO CURING PROCESS

The UV-curing was deeply investigated with three different characterization methods: real-time FTIR, photo-DSC and photo-rheology.
The conversion of the reactive groups was monitored as a function of the irradiation time through a real-time FTIR. As an example, the real-time spectra of BAMF_TMPMP formulation (3 phr of photoinitiator) is reported in **Figure 3**. The area of the peaks related to S-H (2570 cm^{-1}) and C=C (930 cm^{-1}) decreased with the irradiation time confirming the progress of the thiol-ene reaction. Based on the area of the peaks, the conversion was calculated by Eq. 1 and plotted in **Figure 4**. In order to optimize the reactive groups conversion, the influence of the photoinitiator on the UV curing process was assessed. The conversion trend of S-H was investigated by varying the BAPO concentration from 0 to 3 phr as a function of the irradiation time (**Figure 4**). With respect to the BAFM_TMPMP formulation, the increment of the amount of BAPO led to increase final conversion, together with a slight increase of rate of photopolymerization.
This could be due to the increased amount of radical that the photoinitiator generated upon irradiation. More radicals were available to start the polymerization so faster kinetic was achieve and high degree of conversion was reached.
In principle thiol-ene reaction could also be performed without any photoinitiator [48]. However, as faster reactivity and a higher thiol-ene conversion were obtained in the presence of 3 phr of the photoinitaitor then the UV-cured coatings were prepared in the presence of BAPO.
The click characteristic of the reaction [32] was confirmed by comparing the trend of the conversion of the two functional groups as it can be noticed in **Figure 5**. The conversion of the C=C and S-H followed the same tendency meaning that the reaction followed the ratio 1:1 between the two functional group which is the main attribute of the thiol-ene click reaction.

The real-time FTIR analysis were conducted for all formulations and the conversion results are reported in the **Table 2**. As it can be noticed, the final conversion was comparable for all formulations involving both BAMF and BACBDA. The lower value reached for the formulation with BACBDA could be explained considering the higher steric hindrance of the allyl monomer with respect to the formulation bearing BAMF. However, all the value were above 70 % so it is possible to affirm that all the synthetized allyl monomers showed good reactivity to UV-light and good interaction with the thiol-based monomers.

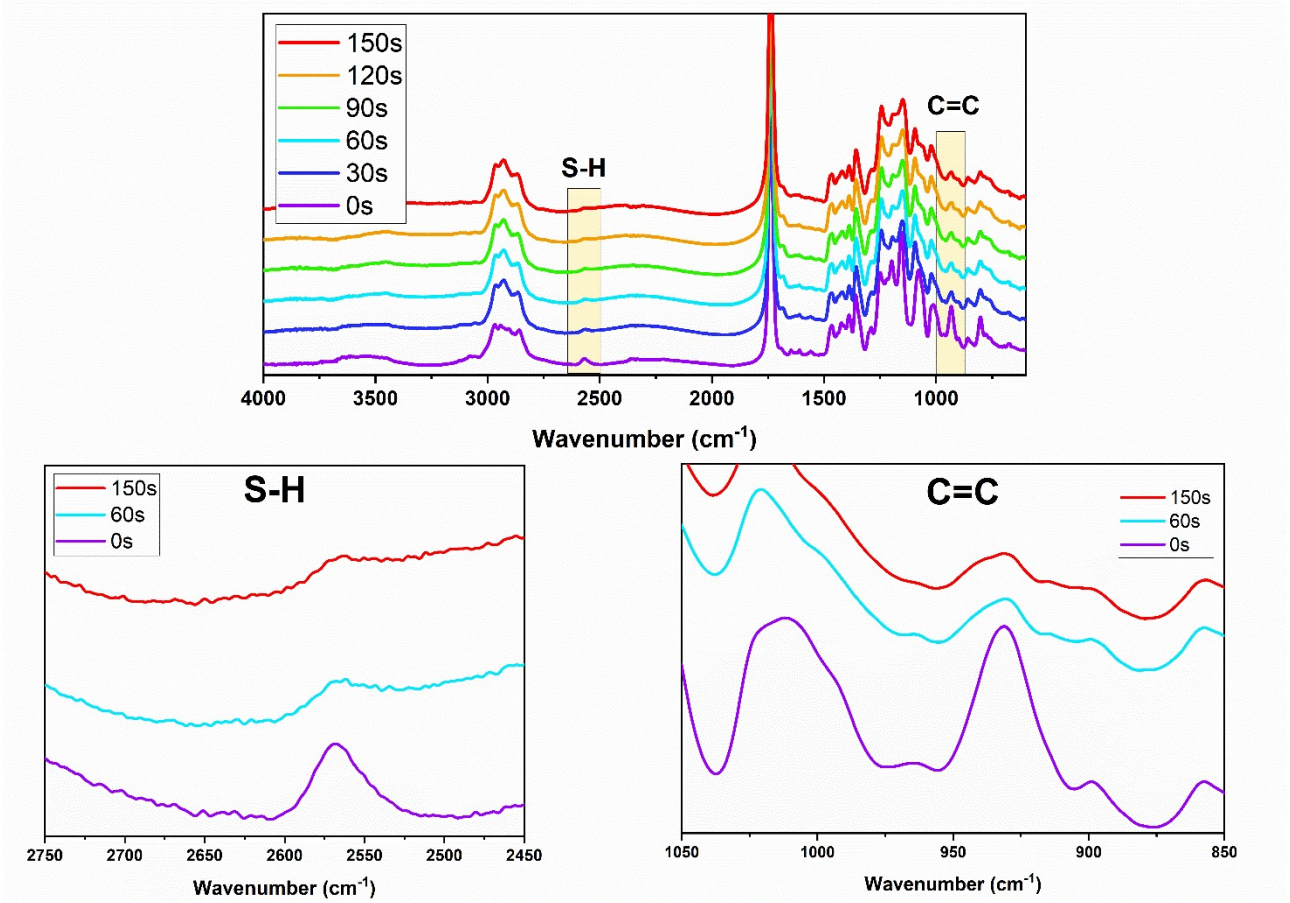

Figure 3. Real time-FITR spectra obtained for BAMF_TMPTP with 3 phr of photoinitiator.

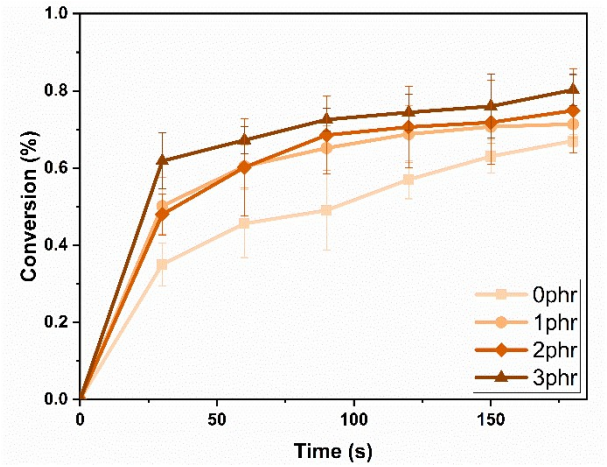

Figure 4. Conversion curves of S-H bond obtained for the BAMF_TMPTP with 0, 1, 2 and 3 phr of BAPO.

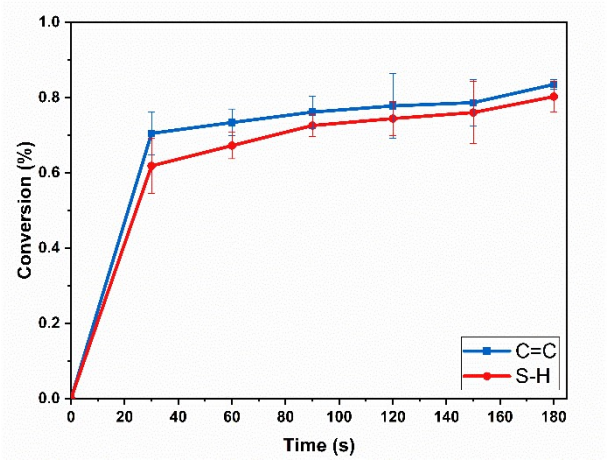

Figure 5. Conversion of functional group in function of the time, C=C is reported in blue while S-H is showed in red. The graph reported the BAMF_TMPMP formulation with 3 phr of photoinitiatior.

Table 2. Conversion evaluated by means of real-time FTIR analysis. All the formulation had 3 phr of BAPO.

ENTRY	Conversion S-H (%)	Conversion C=C (%)
BAMF_TMPMP	80 ± 4	83 ± 1
BAMF_PETMP	75 ± 1	74 ± 1
BACBDA_TMPMP	74 ± 2	77 ± 2
BACBDA_PETMP	72 ± 3	69 ± 5

The FTIR results were confronted with the photo-DSC data. The influence of the amount of photoinitiator was also investigated by means of photo-DSC by evaluating the curing peak. The **Figure 6a** showed the photo-thermograms obtained for BAMF_TMPTP. As it can be noticed, the addition of the photoinitiator had a significant effect of the heat release (ΔH). Indeed, the increase of ΔH after addition of photoinitiator corroborates the previous results with real-time FTIR.
Moreover, the investigation of h_{peak} (peak height at maximum of the DSC curve) revealed that the highest value was reached with 3 phr. The h_{peak} is proven to be proportional to the rate of polymerization so it is possible to affirm the beneficial effect of initiator on the kinetic of the reaction. As last consideration, the t_{peak} (time at maximum rate of polymerization) decreased increasing the amount of photoinitiator. Specifically, it went from 18 s to 10 s passing from 0 phr to 3 phr of photoinitiator corroborating the previous data. As shown in **Figure 6b**, the amount of heat released increased with the amount of photoinitiator corroborating the trend seen for the FT-IR measurement. The maximum ΔH value of 210 J/g was reached for 3 phr of BAPO.
The conversion of all different formulations was calculated (Eq. 2) based on the photo-DSC analysis reposted in **Figure S5** and the results are reported in the **Table 3**. The values were obtained considering 79.5 kJ/mol as theoretical value of heat release for the reaction between an ene and thiol group [49].
The lower degree of conversion reached in the photo-DSC analysis with respect to the real-time FTIR data can be explained considering the different displacement of the sample. In the real-time FTIR, the sample was spread with a thickness of 32 um so there was a negligible effect of the light absorption by the monomer itself and by the formed polymer, while in the DSC pan the effect of light penetration can be seen. In order to explain the possible absorption of the ene-monomers a UV-vis analysis was carried out to evaluate the light absorption. The result is reported in the **Figure S4.** Both monomers showed absorption peak due to the presence of furan ring. However, the BACBDA had higher absorption region with respect to BAMF that can interfere with the UV-light limiting the conversion for bulk polymerization.

In order to verify the possibility to cross-link bulk samples useful for the mechanical characterization, the gel % was carried out on the UV-cured sample to investigate the gel fraction present after the irradiation. The thermoset revealed the highest value for BAMF_TMPMP with 80 ± 2 %; the BAMF_PETMP based thermoset had a value of 78 ± 3 %. The value slightly decreased with the introduction of BACBDA reaching 72 ± 4 % and 68 ± 3 % for the coating bearing TMPMP and PETMP respectively. The lower gel content for the thermoset bearing BACBDA moities confirmed the DSC results and the limitation of the polymerization due to steric hindrance and light penetration. However, the gel% values demonstrated the effective formation of insoluble fraction due to the cross-links between the polymer chains confirming the possibility to create coatings.

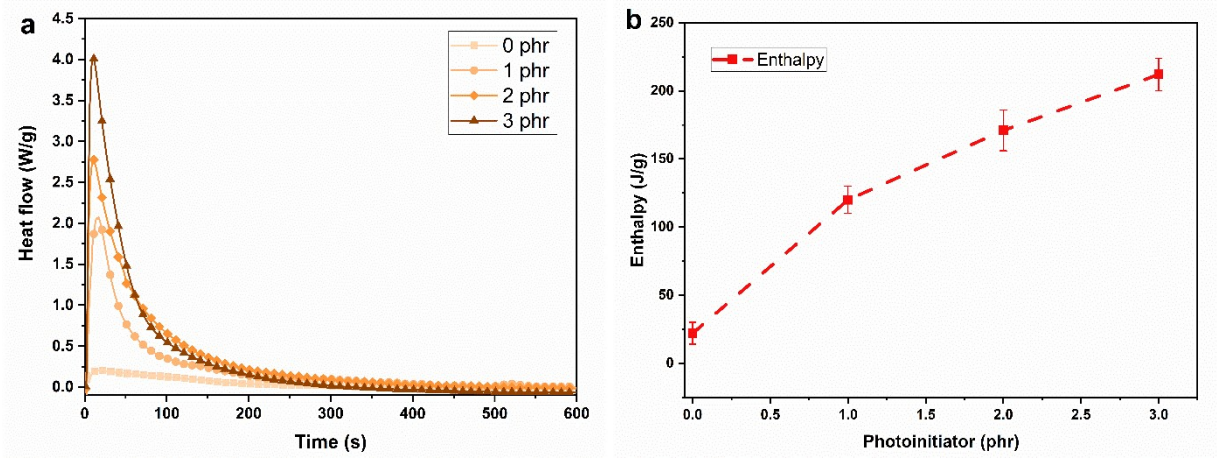

Figure 6. (a) Photo-DSC thermogram for the BAMF_TMPTP with different amount of photoinitiator (0 phr, 1 phr, 2 phr and 3 phr); (b) heat released (*ΔH*) in function of the phr of photoinitiator used.

Table 3. Conversion evaluated by means of real-time FTIR analysis. All the formulation had 3 phr of BAPO.

ENTRY	h_{peak} (W/g)	ΔH_{exp} (J/g)	Conversion[a] (%)
BAMF_TMPMP	3.9 ± 0.4	210 ± 12	62
BAMF_PETMP	4.5 ± 0.5	225 ± 10	64
BACBDA_TMPMP	2.5 ± 0.4	90 ± 13	35
BACBDA_PETMP	3.1 ± 0.8	75 ± 15	28

[a] Conversion of the C=C double bonds by radical crosslinking calculated according to Eq. 2

In addition to real-time FT-IR and photo-DSC, the real-time photorheology was performed to further investigate the photocuring process. In this case the progression of the curing was evaluated considering the trend in the storage modulus and its increment due to the cross-linking reaction. The UV-irradiation led to an increase of storage modulus of the resin upon a plateau when the reaction is terminated. **Figure 7a** shows the result obtained for BAMF_TMPMP and BAMF_PETMP. The difference of the curves is related to the initial induction time of the reaction.
The thermoset bearing BACBDA (**Figure 7b**) showed higher induction time since the increase of the storage modulus had a delay with respect the formulation bearing BAMF. Moreover, both formulations required more time to reach the plateau of storage modulus. After about 360 s the curves of furandimethanol-based network reached a constant value of modulus while the formulation bearing the cyclobutane-based monomer required 900 s. The explanation of this behavior can be attributes to the light adsorption of the ene monomers. Indeed, two processes can happen when UV-light is directed on the sample. The absorption of the light by the photoinitiator, but also the direct absorption of the light from some chromophore's groups present into the structure of the monomers. The first

case generates radicals when the light interacts with the photoinitiator starting the curing reaction while in the second case the light is adsorbed from the monomer and no radicals are generated. Considering the allyl derivatives, it is important to highlight the UV-vis spectra obtained and presented in **Figure 7**. The light absorption can interfere with the UV emitted from the lamp giving less dose available for the formation of the radical species. Thus, the formulations with the BACBDA required a higher induction time to achieve the amount of radiation necessary to start the curing reaction.

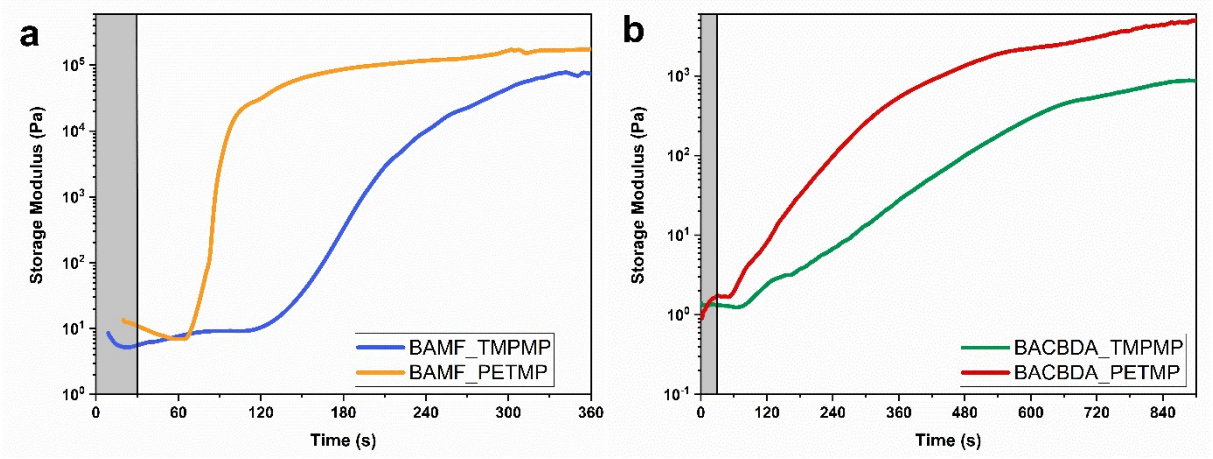

Figure 7. Photo-rheology measurement for the four formulations. (a) BAMF_TMPMP (blue) and BAMF_PETMP (orange); (b) Conversion of the functional group in function of the time, C=C is reported in blue while S-H is showed in red.

3.3. THERMO-MECHANICAL PROPERTIES

The thermomechanical properties of the UV-cured thiol-ene networks were analyzed by DMTA and DSC.

The samples were produced in the same conditions in order to be able to compare the results, the irradiation was guarantee by a DYMAX flood lamp. In **Figure 8** we reported the *Tan δ* curves as a function of the temperature obtained for the investigated formulations. We tried to modulate the thermomechanical properties of the UV-cured coatings by changing the thiol functionalities and the ene structure. Firstly, the different thiols were investigated in BAMF formulations. As observed in **Figure 8**, the UV-cured BAMF_PETMP resin shows higher T_g (-13 °C) compared to BAMF_TMPMP (-26 °C). This result is a direct consequence of tris- and tetra- thiol functionality present in TMPMP and PETMP, respectively. In fact, a higher number of thiol groups were associated with a higher rigidity and T_g of final coating as previously reported [40,50], due to an expected higher crosslinking density.

Thus, the thiol-monomer with four functionalities led to a crosslinked network with a higher glass transition. The high crosslinking density is in accord with the high gel content reported.

The influence of the bis allyl structures were also reported by selecting for BACBDA and BAMF with the same thiol, e.g. TMPMP. Furthermore, comparing the thermomechanical relaxations obtained for BAMF_TMPMP and BACBDA_TMPMP, we observed an increment of T_g around 38 °C when employing BACBDA instead of BAMF. This can be explained evaluating the intrinsic rigidity of the CBDA-2 derivatives bearing a stiff cyclobutane ring. The cyclobutane ring would ensure higher structural stability resulting in better thermo-mechanical properties. The same effect can be observed in bis-allyls_PETMP thermoset. In this case the chemical structure of BACBDA led to an increase of the final *Tg* of about 35 °C with respect to the BAMF.

The T_g of the thiol-ene networks were comparable with the previous studies [37,39,45]. Moreover, the BACBDA_PETMP (T_g = 24 °C) revealed higher *Tg* with respect to other biobased thiol-ene

thermosets derived from ferulic acid [41], isosorbide [37] and eugenol [45]. The evaluation of the cross-link density revealed an increment from BAMF_PETMP to BACBDA_PETMP. The trend in the cross-link density followed the same trend of the T_g. Despite the low conversion the BACBDA_PETMP reached the highest value of the T_g and cross-link density. This result highlights the possibility to have good performance exploiting the rigid chemical structure and high monomer functionality of CBDA-2. The BAMF_TMPMP has a cross-link density value of 61 mmol/dm^3 comparable to the value of BACBDA_TMPMP despite the lower T_g. This can be explained considering the highest level of conversion and the higher gel content reached for the formulation bearing BAMF and TMPMP. As mentioned in the previous chapter, this formulation was the only that overcome the 80 % of conversion leading to high cross-link density. All the results are reported in the **Table 4**.

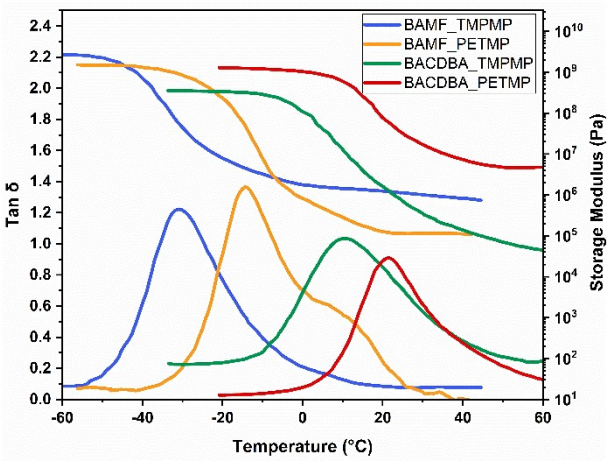

Figure 8. DMTA result for the four different thermosets obtained through thiol-ene chemistry.

The DSC was used to confirm the result of DMTA. The **Figure 9** shows the thermogram obtained for the four different formulations UV-cured in the same conditions and the trend observed in DMTA was confirmed. The BACBDA_PETMP reached the highest T_g value (19 °C) while the FDM_TMPMP had the lowest one with T_g = – 14 °C. All the data are gathered in **Table 4**.

Table 4. Thermo-mechanical properties evaluated by means of DMTA and DSC.

ENTRY	T_g [1] (°C)	T_g [2] (°C)	ν_c [3] (mmol/dm^3)
BAMF_TMPMP	− 26 ± 4	− 14 ± 8	61
BAMF_PETMP	− 13 ± 4	− 3 ± 7	18
BACBDA_TMPMP	+ 12 ± 3	+ 8 ± 5	60
BACBDA_PETMP	+ 24 ± 3	+ 19 ± 4	607

[1] Evaluated by means of DMTA;
[2] Evaluated by means of DSC;
[3] Calculated according Equation 4;

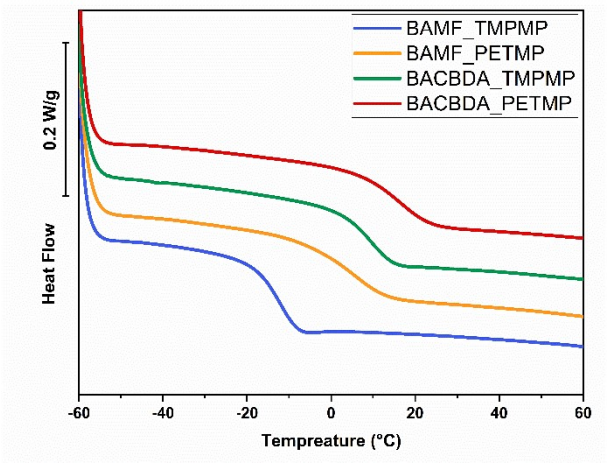

Figure 9. DSC thermograms highlighting the glass transition region from the different UV-cured thermosets.

3.4. TENSILE PROPERTIES

The tensile tests were performed on UV-cured coatings to investigate their mechanical behavior. **Figure 10** shows typical stress-strain curves obtained for the thiol-ene UV-cured networks. The thermosets exhibited elastic behavior with a considerable strain at break that can be explained by the relatively low T_g values reported in **Table 4**. Indeed, in the tested conditions (room temperature) all the bis-allyl coatings were in the rubbery region (above the T_g). A general trend is observed when PETMP is used instead of TMPMP in the bis allyl resins. Indeed, the higher number of thiol functionalities in PETMP allowed to achieve higher elastic modulus and stress at break in the measured samples. This result can be also reconducted to higher T_g reported for bis allyls_PETMP with respect to the bis allyls_TMPMP. The highest stress at break and elastic modulus were reached for BACBDA_PETMP with a value of 9.3×10^5 Pa, and 9.7 MPa, respectively. The tailoring of the tensile properties was verified and corroborated the results obtained for the DMTA analysis. All the data are reported in **Table 5**.

Finally, the evaluation of toughness from the area under the stress-strain curve was carried out. The trend reveals the highest value for BACBDA_PETMP with 11.44 J/m^3 10^4. The BACBDA increase the toughness of the thermoset with respect to the coating bearing BAMF. The higher rigidity of the structure derived from the cyclobutane ring could contribute to affect this property as well as the higher cross-link density reached.

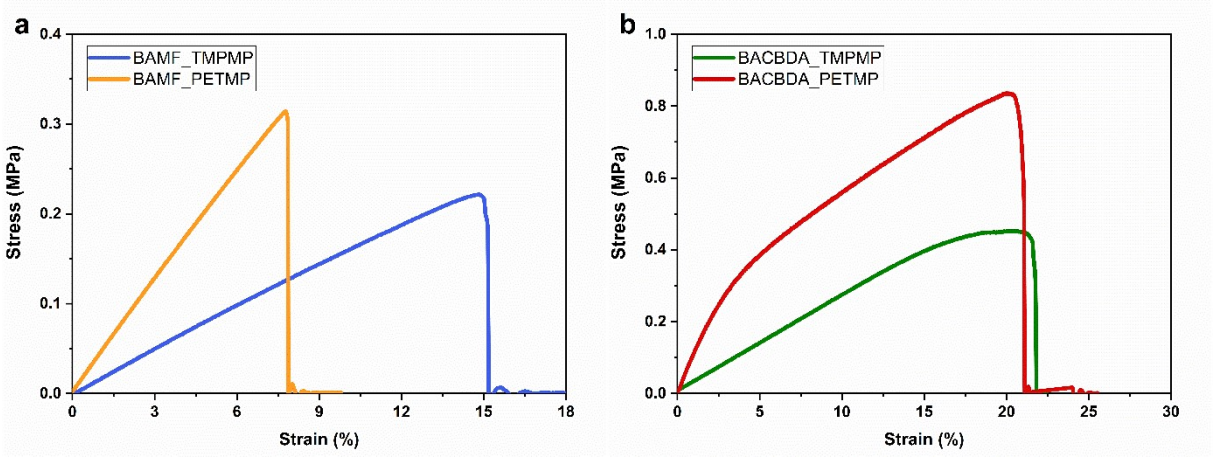

Figure 10. Stress-strain curves for the tested thermoset. (a) Thermoset bearing BAMF; (b) Thermoset produced with BACBDA as ene monomer. The reported curves were the significative ones taken from the 5-replica performed for each thermoset.

Table 5. Mechanical properties evaluated through the tensile test.

ENTRY	*E* (MPa)	*σ at break* (MPa)	*Strain at break* (%)	*Toughness* (J/m^3 10^4)
BAMF_TMPMP	1.7 ± 0.3	0.21 ± 0.02	14.5 ± 0.6	1.33 ± 2.7
BAMF_PETMP	4.1 ± 0.4	0.33 ± 0.06	8.5 ± 1.3	1.78 ± 5.0
BACBDA_TMPMP	2.2 ± 0.3	0.37 ± 0.07	20.5 ± 0.8	4.83 ± 5.6
BACBDA_PETMP	9.7 ± 1.3	0.93 ± 0.13	20.8 ± 1.3	11.44 ± 3.23

3.5. COATING PROPERTIES

The surface properties of the UV-cured coatings were tested and reported in **Table 6**. Contact angle measurements were done showing similar value for all the tested samples. In particular, the hydrophobicity of the surface increased when using thiol from TMPMP to PETMP and when using bis-allyl from BAMF to BACBDA. The chemical structure could be a reason for this change but also the low conversion of thiol groups could increase the contact angle of the surface [51]. Instead, considering the hardness, the presence of the PETMP, tetrafunctional thiol, increase the hardness with respect to the same thermoset bearing TMPMP. Such difference this could be explained by the higher T_g reached by PETMP samples.

Table 6. Contact angle and hardness of the coatings.

ENTRY	*Contact angle* (°)	Hardness (HL)
BAMF_TMPMP	62 ± 4	156 ± 12
BAMF_PETMP	66 ± 3	245 ± 29
BACBDA_TMPMP	72 ± 2	195 ± 23
BACBDA_PETMP	74 ± 4	296 ± 33

4. CONCLUSION

The present study investigated UV-induced cross-linking of furan-based allyl monomers exploiting the thiol-ene chemistry. The synthesis of biobased allyl derivatives opened the possibility to move toward green and sustainable alternative to the commercial monomers. The exploitation of different furan derivatives, FDM and CBDA-2, gave the possibility to tailor the final properties of the coating due to the different chemical structure of the base monomers. The high rigidity of CBDA-2 derivative structure allowed to reach better thermos-mechanical properties. Moreover, the use of different thiol increased the spectrum of the achievable properties playing with the number of the thiol-functionalities bearing in the thiol monomer involved in the network formation.
The UV-curing was deeply investigated by FTIR, photorheology demonstrating a good reactivity of the synthesized ene monomers with the commercial thiols. The conversion achieved was high for all investigated formulation reaching value above 70 %. The UV-cured coatings were characterized from thermo- to mechanical-properties revealing comparable or even better properties with previous studied of the same field. Indeed, the T_g achieved for the thermosets, especially for the BACBDA_PETMP (T_g = 24 °C), were comparable or even better to previous ones.
In conclusion, we demonstrated the possibility to develop new green alternative based on furan derivatives in the field of coating applications.

BIBLIOGRAPHY

[1] J.J. Bozell, G.R. Petersen, Technology development for the production of biobased products from biorefinery carbohydrates—the US Department of Energy's "Top 10" revisited, Green Chem. 12 (2010) 539–554. https://doi.org/10.1039/B922014C.

[2] L.A. Zevallos Torres, A. Lorenci Woiciechowski, V.O. de Andrade Tanobe, S.G. Karp, L.C. Guimarães Lorenci, C. Faulds, C.R. Soccol, Lignin as a potential source of high-added value compounds: A review, J. Clean. Prod. 263 (2020). https://doi.org/10.1016/j.jclepro.2020.121499.

[3] L. Pezzana, E. Malmström, M. Johansson, M. Sangermano, UV-Curable Bio-Based Polymers Derived from Industrial Pulp and Paper Processes, Polym. . 13 (2021). https://doi.org/10.3390/polym13091530.

[4] A. Gandini, Polymers from renewable resources: A challenge for the future of macromolecular materials, Macromolecules. 41 (2008) 9491–9504. https://doi.org/10.1021/ma801735u.

[5] M.N. Belgacem, A. Gandini, Monomers, polymers and composites from renewable resources, Elsevier, 2011.

[6] K.J. Zeitsch, The chemistry and technology of furfural and its many by-products, Elsevier, 2000.

[7] Y. Lee, J. Lee, Polymers Derived from Hemicellulosic Parts of Lignocellulosic Biomass, Rev. Environ. Sci. Bio/Technology. 18 (2019) 317–334. https://doi.org/10.1007/s11157-019-09495-z.

[8] A. Gandini, Monomers and Macromonomers from Renewable Resources, Biocatal. Polym. Chem. (2010) 1–33. https://doi.org/https://doi.org/10.1002/9783527632534.ch1.

[9] A. Gandini, M.N. Belgacem, Chapter 6 - Furan Derivatives and Furan Chemistry at the Service of Macromolecular Materials, in: M.N. Belgacem, A.B.T.-M. Gandini Polymers and Composites from Renewable Resources (Eds.), Elsevier, Amsterdam, 2008: pp. 115–152. https://doi.org/https://doi.org/10.1016/B978-0-08-045316-3.00006-5.

[10] Y. Román-Leshkov, J.N. Chheda, J.A. Dumesic, Phase modifiers promote efficient production of hydroxymethylfurfural from fructose, Science (80-.). 312 (2006) 1933–1937.

[11] E. Taarning, I.S. Nielsen, K. Egeblad, R. Madsen, C.H. Christensen, Chemicals from Renewables: Aerobic Oxidation of Furfural and Hydroxymethylfurfural over Gold Catalysts, ChemSusChem. 1 (2008) 75–78. https://doi.org/https://doi.org/10.1002/cssc.200700033.

[12] A. Gandini, M.N. Belgacem, Furan resins, INC, 2021. https://doi.org/10.1016/B978-0-12-821632-3.00006-3.

[13] N. Guigo, A. Mija, L. Vincent, N. Sbirrazzuoli, Eco-friendly composite resins based on renewable biomass resources: Polyfurfuryl alcohol/lignin thermosets, Eur. Polym. J. 46 (2010) 1016–1023. https://doi.org/https://doi.org/10.1016/j.eurpolymj.2010.02.010.

[14] H.A.S. Valentino, P. de Tarso Laia dos Reis e Silva Pupio, A. Gandini, T.M. Lacerda, Furfuryl alcohol/tung oil matrix-based composites reinforced with bacterial cellulose fibres, Cellulose. 28 (2021) 7109–7121. https://doi.org/10.1007/s10570-021-03999-0.

[15] L. Pezzana, G. Melilli, G. Nathanaël, N. Sbirrazzuoli, M. Sangermano, Cationic UV Curing of Bioderived Epoxy Furan-Based Coatings: Tailoring the Final Properties by In Situ Formation of Hybrid Network and Addition of Monofunctional Monomer, ACS Sustain. Chem. Eng. (2021). https://doi.org/10.1021/acssuschemeng.1c06939.

[16] A. Marotta, N. Faggio, V. Ambrogi, P. Cerruti, G. Gentile, A. Mija, Curing Behavior and Properties of Sustainable Furan-Based Epoxy/Anhydride Resins, Biomacromolecules. 20 (2019) 3831–3841. https://doi.org/10.1021/acs.biomac.9b00919.

[17] A. Codou, M. Moncel, J.G. van Berkel, N. Guigo, N. Sbirrazzuoli, Glass transition dynamics and cooperativity length of poly(ethylene 2,5-furandicarboxylate) compared to poly(ethylene terephthalate), Phys. Chem. Chem. Phys. 18 (2016) 16647–16658.

https://doi.org/10.1039/C6CP01227B.
[18] A. Eerhart, A.P.C. Faaij, M.K. Patel, Replacing fossil based PET with biobased PEF; process analysis, energy and GHG balance, Energy Environ. Sci. 5 (2012) 6407–6422.
[19] E. de Jong, M.A. Dam, L. Sipos, G.-J.M. Gruter, Furandicarboxylic Acid (FDCA), A Versatile Building Block for a Very Interesting Class of Polyesters, in: Biobased Monomers, Polym. Mater., American Chemical Society, 2012: p. 1. https://doi.org/doi:10.1021/bk-2012-1105.ch001.
[20] A.F. Sousa, R. Patrício, Z. Terzopoulou, D.N. Bikiaris, T. Stern, J. Wenger, K. Loos, N. Lotti, V. Siracusa, A. Szymczyk, S. Paszkiewicz, K.S. Triantafyllidis, A. Zamboulis, M.S. Nikolic, P. Spasojevic, S. Thiyagarajan, D.S. Van Es, N. Guigo, Recommendations for replacing PET on packaging, fiber, and film materials with biobased counterparts, Green Chem. 23 (2021) 8795–8820. https://doi.org/10.1039/d1gc02082j.
[21] S. Rajagopalan, Preparation of β, 2-furyl acrylic acid, in: Proc. Indian Acad. Sci. A, Springer, 1942: pp. 163–166.
[22] Z. Wang, M. Scheuring, M. Mabin, R. Shahni, Z.D. Wang, A. Ugrinov, J. Butz, Q.R. Chu, Renewable Cyclobutane-1, 3-dicarboxylic Acid (CBDA) Building Block Synthesized from Furfural via Photocyclization, ACS Sustain. Chem. Eng. 8 (2020) 8909–8917.
[23] A.C. Fonseca, M.S. Lima, A.F. Sousa, A.J. Silvestre, J.F.J. Coelho, A.C. Serra, Cinnamic acid derivatives as promising building blocks for advanced polymers: Synthesis, properties and applications, Polym. Chem. 10 (2019) 1696–1723. https://doi.org/10.1039/c9py00121b.
[24] D. Tunc, C. Le Coz, M. Alexandre, P. Desbois, P. Lecomte, S. Carlotti, Reversible cross-linking of aliphatic polyamides bearing thermo- and photoresponsive cinnamoyl moieties, Macromolecules. 47 (2014) 8247–8254. https://doi.org/10.1021/ma502083p.
[25] J.P. Chesterman, F. Chen, A.J. Brissenden, B.G. Amsden, Synthesis of cinnamoyl and coumarin functionalized aliphatic polycarbonates, Polym. Chem. 8 (2017) 7515–7528. https://doi.org/10.1039/c7py01195d.
[26] Z. Wang, B. Miller, M. Mabin, R. Shahni, Z.D. Wang, A. Ugrinov, Q.R. Chu, Cyclobutane-1,3-Diacid (CBDA): A Semi-Rigid Building Block Prepared by [2+2] Photocyclization for Polymeric Materials, Sci. Rep. 7 (2017) 1–7. https://doi.org/10.1038/s41598-017-13983-z.
[27] J. Tellers, N. Sbirrazzuoli, N. Guigo, A rigid plant oil-based thermoset with a furfural-derived cyclobutane cross-linker, Green Chem. 23 (2021) 8053–8060. https://doi.org/10.1039/d0gc04323k.
[28] M. Sangermano, N. Razza, J.V. Crivello, Cationic UV-curing: Technology and applications, Macromol. Mater. Eng. 299 (2014) 775–793. https://doi.org/10.1002/mame.201300349.
[29] Y. Yagci, Photoinitiated cationic polymerization of unconventional monomers, Macromol. Symp. 240 (2006) 93–101. https://doi.org/10.1002/masy.200650812.
[30] N.B. Cramer, C.N. Bowman, Kinetics of thiol-ene and thiol-acrylate photopolymerizations with real-time Fourier transform infrared, J. Polym. Sci. Part A Polym. Chem. 39 (2001) 3311–3319. https://doi.org/10.1002/pola.1314.
[31] C.E. Hoyle, C.N. Bowman, Thiol-ene click chemistry, Angew. Chemie - Int. Ed. 49 (2010) 1540–1573. https://doi.org/10.1002/anie.200903924.
[32] A.B. Lowe, Thiol-ene "click" reactions and recent applications in polymer and materials synthesis, Polym. Chem. 1 (2010) 17–36. https://doi.org/10.1039/b9py00216b.
[33] M. Claudino, J.M. Mathevet, M. Jonsson, M. Johansson, Bringing d-limonene to the scene of bio-based thermoset coatings via free-radical thiol-ene chemistry: Macromonomer synthesis, UV-curing and thermo-mechanical characterization, Polym. Chem. 5 (2014) 3245–3260. https://doi.org/10.1039/c3py01302b.
[34] A. Stamm, M. Tengdelius, B. Schmidt, J. Engström, P.O. Syrén, L. Fogelström, E. Malmström, Chemo-enzymatic pathways toward pinene-based renewable materials, Green Chem. 21 (2019) 2720–2731. https://doi.org/10.1039/C9GC00718K.
[35] A.C. Weems, K.R. Delle Chiaie, J.C. Worch, C.J. Stubbs, A.P. Dove, Terpene- and

terpenoid-based polymeric resins for stereolithography 3D printing, Polym. Chem. 10 (2019) 5959–5966. https://doi.org/10.1039/c9py00950g.
[36] E. Çakmakçi, F. Şen, M.V. Kahraman, Isosorbide Diallyl Based Antibacterial Thiol-Ene Photocured Coatings Containing Polymerizable Fluorous Quaternary Phosphonium Salt, ACS Sustain. Chem. Eng. 7 (2019) 10605–10615. https://doi.org/10.1021/acssuschemeng.9b01161.
[37] L. Pezzana, M. Sangermano, Fully biobased UV-cured thiol-ene coatings, Prog. Org. Coatings. 157 (2021) 106295.
[38] T.S. Kristufek, S.L. Kristufek, L.A. Link, A.C. Weems, S. Khan, S.M. Lim, A.T. Lonnecker, J.E. Raymond, D.J. Maitland, K.L. Wooley, Rapidly-cured isosorbide-based cross-linked polycarbonate elastomers, Polym. Chem. 7 (2016) 2639–2644. https://doi.org/10.1039/c5py01659b.
[39] L. Pezzana, M. Mousa, E. Malmström, M. Johansson, M. Sangermano, Bio-based monomers for UV-curable coatings: allylation of ferulic acid and investigation of photocured thiol-ene network, Prog. Org. Coatings. 150 (2021) 105986. https://doi.org/https://doi.org/10.1016/j.porgcoat.2020.105986.
[40] D.B. Larsen, R. Sønderbæk-Jørgensen, J.Ø. Duus, A.E. Daugaard, Investigation of curing rates of bio-based thiol-ene films from diallyl 2,5-furandicaboxylate, Eur. Polym. J. 102 (2018) 1–8. https://doi.org/https://doi.org/10.1016/j.eurpolymj.2018.03.005.
[41] L. Pezzana, G. Melilli, N. Guigo, N. Sbirrazzuoli, M. Sangermano, Cross-Linking of Biobased Monofunctional Furan Epoxy Monomer by Two Steps Process, UV Irradiation and Thermal Treatment, Macromol. Chem. Phys. n/a (2022) 2200012. https://doi.org/https://doi.org/10.1002/macp.202200012.
[42] L. Cottier, G. Descotes, Y. Soro, Heteromacrocycles from Ring-Closing Metathesis of Unsaturated Furanic Ethers, Synth. Commun. 33 (2003) 4285–4295. https://doi.org/10.1081/SCC-120026858.
[43] T. Engel, G. Kickelbick, Furan-Modified Spherosilicates as Building Blocks for Self-Healing Materials, Eur. J. Inorg. Chem. 2015 (2015) 1226–1232. https://doi.org/https://doi.org/10.1002/ejic.201402551.
[44] Z.D. Wang, Q. Elliott, Z. Wang, R.A. Setien, J. Puttkammer, A. Ugrinov, J. Lee, D.C. Webster, Q.R. Chu, Furfural-Derived Diacid Prepared by Photoreaction for Sustainable Materials Synthesis, ACS Sustain. Chem. Eng. 6 (2018) 8136–8141. https://doi.org/10.1021/acssuschemeng.8b02415.
[45] T. Yoshimura, T. Shimasaki, N. Teramoto, M. Shibata, Bio-based polymer networks by thiol-ene photopolymerizations of allyl-etherified eugenol derivatives, Eur. Polym. J. 67 (2015) 397–408. https://doi.org/10.1016/j.eurpolymj.2014.11.013.
[46] ASTM, Standard Test Method for Tensile Properties of Thin Plastic Sheeting, ASTM International, Www.Astm.Org. (2002) 1–12. https://doi.org/10.1520/D0882-18.
[47] ASTM D3363-05, Standard Test Method for Film Hardness by Pencil Test, ASTM Int. (2005). https://doi.org/10.1520/D3363-05.
[48] N.B. Cramer, J.P. Scott, C.N. Bowman, Photopolymerizations of Thiol−Ene Polymers without Photoinitiators, Macromolecules. 35 (2002) 5361–5365. https://doi.org/10.1021/ma0200672.
[49] B.H. Northrop, R.N. Coffey, Thiol-ene click chemistry: Computational and kinetic analysis of the influence of alkene functionality, J. Am. Chem. Soc. 134 (2012) 13804–13817. https://doi.org/10.1021/ja305441d.
[50] I. Ribca, M.E. Jawerth, C.J. Brett, M. Lawoko, M. Schwartzkopf, A. Chumakov, S. V Roth, M. Johansson, Exploring the Effects of Different Cross-Linkers on Lignin-Based Thermoset Properties and Morphologies, ACS Sustain. Chem. Eng. 9 (2021) 1692–1702. https://doi.org/10.1021/acssuschemeng.0c07580.
[51] S. Nameer, S. Semlitsch, M. Martinelle, M. Johansson, One-pot enzyme-catalyzed synthesis

of dual-functional polyester macromers towards surface-active hydrophobic films, RSC Adv. 7 (2017) 50294–50299. https://doi.org/10.1039/C7RA09828F.

SUPPORTING INFO

^{13}C NMR (101 MHz, DMSO) δ 151.74, 134.84, 116.72, 110.12, 70.03, 63.28.

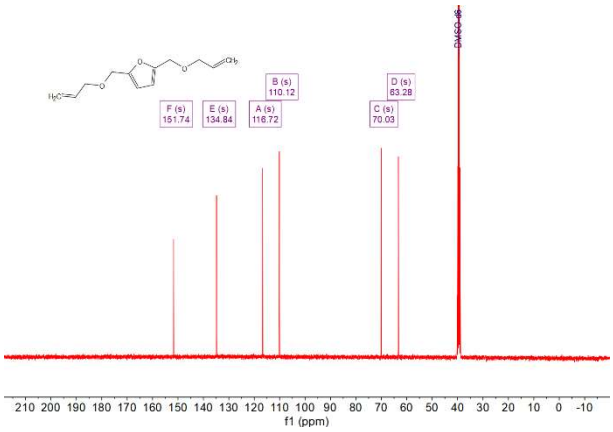

Figure S1. ^{13}C NMR of BAMF in DMSO-d_6.

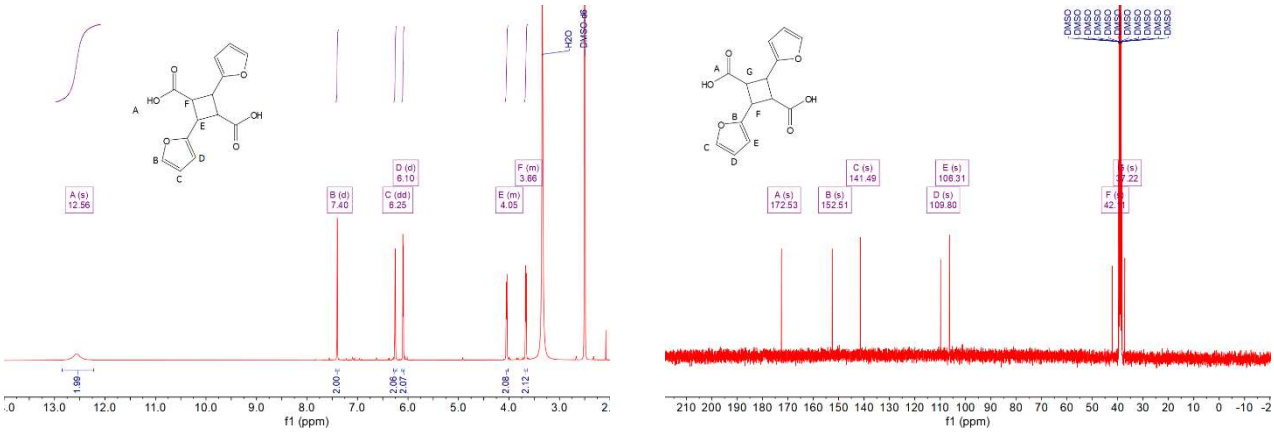

Figure S2. 1H NMR of CBDA-2 (left) and 13C NMR (right) in DMSO-d_6.

^{13}C NMR (101 MHz, DMSO) δ 171.05, 152.36, 142.22, 132.26, 118.13, 110.36, 107.14, 65.08, 42.30, 37.84.

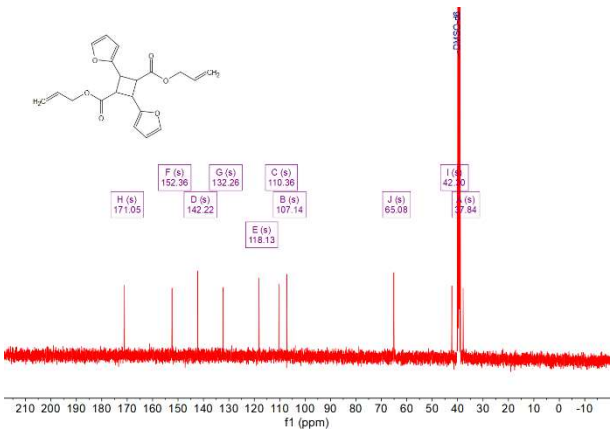

Figure S3. ^{13}C NMR of BACBDA in DMSO-d_6

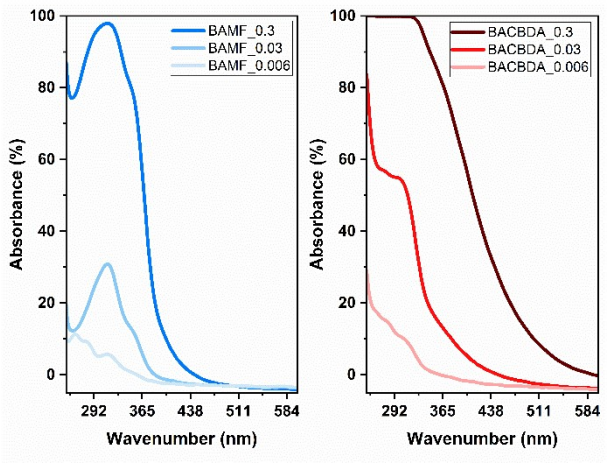

Figure S4. UV-vis spectra of furan-based ene monomers. BAMF is reported in blue while BACBDA is reported in red. The monomers were tested at three different concentrations.

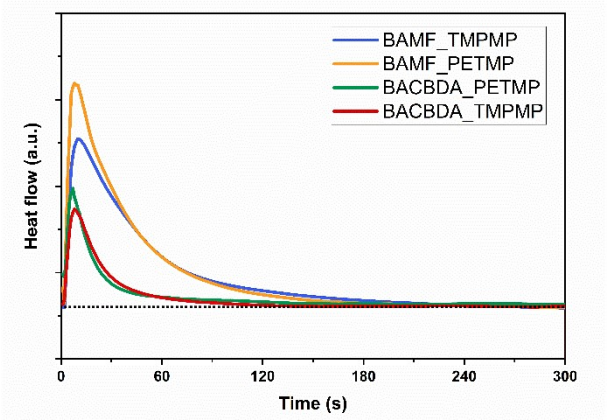

Figure S5. Thermogram of UV-curing for the tested formulation at 25 °C.